IOPscience iopscience.iop.org

Home Search Collections Journals About Contact us My IOPscience

A global (volume averaged) model of a nitrogen discharge: I. Steady state

This content has been downloaded from IOPscience. Please scroll down to see the full text.

2009 Plasma Sources Sci. Technol. 18 045001

(http://iopscience.iop.org/0963-0252/18/4/045001)

View the table of contents for this issue, or go to the journal homepage for more

Download details:

IP Address: 132.239.1.230
This content was downloaded on 14/01/2015 at 20:11

Please note that terms and conditions apply.

Plasma Sources Sci. Technol. **18** (2009) 045001 (15pp) doi:10.1088/0963-0252/18/4/045001

A global (volume averaged) model of a nitrogen discharge: I. Steady state

E G Thorsteinsson[1,2] **and J T Gudmundsson**[1,2]

[1] Department of Electrical and Computer Engineering, University of Iceland, Hjardarhaga 2-6, IS–107 Reykjavik, Iceland
[2] Science Institute, University of Iceland, Dunhaga 3, IS–107 Reykjavik, Iceland

E-mail: tumi@hi.is

Received 26 November 2008, in final form 8 April 2009
Published 31 July 2009
Online at stacks.iop.org/PSST/18/045001

Abstract
A global (volume averaged) model is developed for a nitrogen discharge in the steady state for the pressure range 1–100 mTorr. The electron energy distribution function is allowed to vary from a Maxwellian to a Druyvesteyn distribution. Varying the electron energy distribution function from a Maxwellian-like to a Druyvesteyn-like influences mainly the density of excited species, ground state species being more important when the distribution is Druyvesteyn-like. We find that the nitrogen discharge is essentially atomic when the pressure is around 1 mTorr and is highly molecular when the pressure is 100 mTorr. The relative reaction rates for the creation and destruction of nitrogen atoms and atomic ions are explored over the pressure range of interest. The model calculations are compared with measurements found in the literature. There is excellent agreement between the model and the measurements for the electron and ion densities as well as the electron temperature. However, a large discrepancy between the model predictions and the measurements of the nitrogen atom density remains unexplained.

(Some figures in this article are in colour only in the electronic version)

1. Introduction

Low pressure nitrogen discharges have a wide range of applications, particularly within the semiconductor industry. They are used as an N atom source for the growth of semiconducting III–V nitrides by plasma assisted molecular beam epitaxy [1, 2]. The Ar/N_2 discharge is applied in reactive magnetron sputtering to grow nitrides such as TiN thin films [3]. Nitridation processes are applied to form high quality oxynitride films to act as a boron diffusion barrier for the gate oxide [4]. More recently a mixture of N_2/H_2 is used to etch organic films with low dielectric constant [5]. Nitrogen discharges are also employed in surface post-processing of various metals and alloys. Plasma nitriding is used as an economical method to improve hardness, corrosion, wear resistance and surface quality of stainless steel [6, 7]. Additionally, plasma ion implantation of nitrogen is used to substantially reduce the wear rate of various alloys [8, 9], commonly increasing the lifetime by 2–3 orders of magnitude.

The volume averaged global model for high density discharges was developed by Lieberman and Gottscho [10] for noble gases and extended to molecular gases by Lee *et al* [11] and Lee and Lieberman [12]. A more elaborate volume averaged global model of O_2 [13–16] and Ar/O_2 mixture [17–19] has been developed. The main idea of a global model is to neglect the complexity which arises when spatial variations are considered and to generate a model that encompasses a large number of reactions in order to model a processing plasma with a limited computing power. Thus the model does not describe spatial distribution but captures scalings of plasma parameters with control parameters. The model allows us to investigate various phenomena, such as the effects of excited species, negative ions and particular reactions on the overall discharge.

Here we develop a global model of the nitrogen discharge for the pressure regime 1–100 mTorr in the steady state. A detailed model of the plasma chemistry is developed, and the reaction rates explored for various conditions. The electron energy distribution function is allowed to vary from a Maxwellian-like distribution to a Druyvesteyn-like distribution. We explore, in particular, dissociation of the nitrogen molecule, the creation and loss of the nitrogen

 © 2009 IOP Publishing Ltd Printed in the UK

atom and the atomic ion N^+. The nitrogen discharge is an electropositive discharge and the charged particle losses are expected to be mainly at the chamber walls. This work is followed by a study of the plasma dynamics in a pulsed nitrogen discharge [20].

2. The global (volume averaged) model

We assume a cylindrical stainless steel chamber of radius R and length L. A steady flow Q of neutral species is introduced through the inlet. The content of the chamber is assumed to be nearly spatially uniform and the power deposited uniformly into the plasma bulk. The discharge pressure, calculated as the sum of all partial pressures according to the ideal gas law, is adjusted by means of an outlet-flow pressure that partially controls the pumping of gas out of the chamber. The discharge is assumed to consist of 15 species of nitrogen; the seven lowest lying vibrational levels of the ground state nitrogen molecule $N_2(X\,^1\Sigma_g^+, v = 0-6)$, the metastable nitrogen molecule $N_2(A\,^3\Sigma_u^+)$, the ground state nitrogen atom $N(^4S)$, the metastable nitrogen atoms $N(^2D)$ and $N(^2P)$ and the ions N_2^+, N^+, N_3^+ and N_4^+. The electrons are generally assumed to have a Maxwellian-like energy distribution in the range 1–10 eV, but the electron energy distribution function will also be allowed to change to a Druyvesteyn distribution in this study.

2.1. The electron energy distribution function

For a low pressure (<30 mTorr) inductively coupled discharge, measurements have shown that the electron energy distribution is close to being Maxwellian-like in molecular gases, such as in N_2 and O_2 discharges [17, 21, 22]. For higher pressure there are relatively fewer high energy electrons, and the electron energy distribution more resembles the Druyvesteyn distribution [22]. Furthermore, a hole at 3 eV is often observed in the electron energy distribution of the nitrogen discharge, attributed to the strong vibrational loss property of nitrogen discharges [22]. Because of these variations, it is important to evaluate the sensitivity of the plasma parameters to the choice of the electron energy distribution function. Thus, in this study the electron energy distribution function is allowed to vary according to the general distribution function given by [23, 24]

$$f(\mathcal{E}) = c_1 \mathcal{E}^{1/2} \exp(-c_2 \mathcal{E}^x), \tag{1}$$

where $x = 1$ corresponds to the Maxwellian distribution and $x = 2$ to the Druyvesteyn distribution. The coefficients c_1 and c_2 depend on the electron energy $\mathcal{E}$ and the distribution parameter x, and are given as [24]

$$c_1 = \frac{x}{\langle\mathcal{E}\rangle^{3/2}} \frac{[\Gamma(\xi_2)]^{3/2}}{[\Gamma(\xi_1)]^{5/2}}, \tag{2}$$

$$c_2 = \frac{1}{\langle\mathcal{E}\rangle^x} \left[\frac{\Gamma(\xi_2)}{\Gamma(\xi_1)}\right]^x, \tag{3}$$

where $\langle\mathcal{E}\rangle = \frac{3}{2} eT_e$ is the average electron energy and $\Gamma(\xi)$ is the gamma function with $\xi_1 = 3/2x$ and $\xi_2 = 5/2x$. The rate coefficients for electron impact reactions are found by averaging the corresponding cross section, $\sigma(\mathcal{E})$, over the assumed distribution function,

$$k(T_e) = \left(\frac{2, e}{m_e}\right)^{1/2} \int_0^\infty \sigma(\mathcal{E}) \mathcal{E}^{1/2} f(\mathcal{E})\, \mathrm{d}\mathcal{E}. \tag{4}$$

The rate coefficient is calculated with trapezoidal numerical integration for 1000 equally spaced values of T_e in the range 1–10 V and then fitted to the modified Arrhenius form,

$$k(T_e) = A \times T_e^B \times \exp(-C/T_e^x). \tag{5}$$

With the electron energy distribution function given by equation (1), the Bohm velocity is given as [24]

$$u_B = \langle\mathcal{E}\rangle^{1/2} \left(\frac{2}{m_i}\right)^{1/2} \frac{[\Gamma(\xi_1)]}{[\Gamma(\xi_2)\Gamma(\xi_3)]^{1/2}}, \tag{6}$$

where $\xi_3 = 1/2x$. The mean kinetic energy lost per ion lost is given by [24]

$$\mathcal{E}_i = \frac{[\Gamma(\xi_1)]^2}{\Gamma(\xi_2)\Gamma(\xi_3)} \langle\mathcal{E}\rangle + V_s \tag{7}$$

and the mean kinetic energy lost per electron lost is given by [24]

$$\mathcal{E}_e = \frac{\Gamma(\xi_1)\Gamma(\xi_5)}{\Gamma(\xi_2)\Gamma(\xi_4)} \langle\mathcal{E}\rangle, \tag{8}$$

where $\xi_5 = 3/x$. The sheath potential, V_s, can be determined accurately by equating the ion and electron flux at the wall, $\Gamma_e = \Gamma_i$. When the electron energy distribution is Maxwellian-like, V_s has a known analytical solution. If $x > 1$ the accurate solution of V_s can only be determined numerically by iteration of

$$\frac{4 n_i u_B}{n_e \bar{v}_e c_1} = \int_0^1 u^{1/2} \exp(-c_2[u + V_s]^x)\, \mathrm{d}u + \int_0^1 t^{-5/2} \exp(-c_2[t^{-1} + V_s]^x)\, \mathrm{d}t, \tag{9}$$

where $u = \mathcal{E} - V_s$ and $t = (\mathcal{E} - V_s)^{-1}$. The singularity at $t \to 0$ (infinite energy) can be eliminated by observing that the second integral approaches zero when $t \to 0$. In an attempt to find an approximate expression for the sheath potential, a heuristic solution was developed to account for its dependence of the electron energy distribution parameter x. By fitting the accurate solution of V_s in an argon discharge, i.e. where $n_i = n_e$, to a simple power law dependence of x, we arrive at

$$V_s = -T_e \ln\left(4 \frac{n_i u_B}{n_e \bar{v}_e}\right) x^{-0.43}. \tag{10}$$

This simple expression is accurate to within 1.5% from the numerical solution (equation (9)), which is certainly good enough for this study.

2.2. Particle and power balance

The plasma chemistry is described by a set of nonlinear first order differential equations; a particle balance equation for each of the species included in the discharge and a single

equation describing the conservation of energy [11, 13]. The particle balance equation for a species X is given as

$$\frac{\mathrm{d}n^{(X)}}{\mathrm{d}t} = 0 = \sum_i R^{(X)}_{\mathrm{Generation},i} - \sum_i R^{(X)}_{\mathrm{Loss},i}, \qquad (11)$$

where $R^{(X)}_{\mathrm{Generation},i}$ and $R^{(X)}_{\mathrm{Loss},i}$, respectively, are the reaction rates of the various generation and loss processes of the species X. In this study we consider various processes for the loss and generation of the discharge species; volumetric processes are discussed in section 2.4, surface processes in section 2.5 and the pumping of gas in and out of the chamber in section 2.6. For this study the system of first order differential equations is allowed to reach a steady state, i.e. $\mathrm{d}/\mathrm{d}t = 0$. The reaction rate R for a given reaction is calculated as the product of the reactants' densities and the rate coefficient k of the reaction,

$$R = k \times \prod_i n_{\mathrm{r},i} \qquad (\mathrm{m^{-3}\,s^{-1}}) \qquad (12)$$

where $n_{\mathrm{r},i}$ is the density of the ith reactant. Since the discharge is assumed to be quasi-neutral,

$$n_\mathrm{e} = \sum_\mathrm{i} Z_\mathrm{i} n_\mathrm{i}, \qquad (13)$$

where Z_i is the charge of ion i, an equation describing the particle balance of free electrons is not required.

The power balance equation, which equates the absorbed power P_abs to power losses due to elastic and inelastic collisions and losses due to charged particle flow to the walls is given as [25]

$$\frac{1}{V}\left[P_\mathrm{abs} - eVn_\mathrm{e}\sum_\alpha n^{(\alpha)}\mathcal{E}^{(\alpha)}_\mathrm{c}k^{(\alpha)}_\mathrm{iz} - eu_\mathrm{B}n_\mathrm{i}A_\mathrm{eff}(\mathcal{E}_\mathrm{i}+\mathcal{E}_\mathrm{e})\right] = \frac{\mathrm{d}}{\mathrm{d}t}\left(\frac{3}{2}en_\mathrm{e}T_\mathrm{e}\right) = \frac{\mathrm{d}}{\mathrm{d}t}\left(\frac{3}{2}p_\mathrm{e}\right) = 0 \qquad (14)$$

where p_e is the thermal electron energy density, V is the volume of the discharge chamber, A_eff is the effective area for ion loss given in section 2.5 by equation (26) and u_B is the Bohm velocity given by equation (6). $\mathcal{E}_\mathrm{i}$ and $\mathcal{E}_\mathrm{e}$ are the mean kinetic energy lost per ion and per electron lost, given by equations (7) and (8), respectively. The sum is over all ground state neutral particles α, having density $n^{(\alpha)}$, ionization rate coefficient $k^{(\alpha)}_\mathrm{iz}$ and collisional energy loss per electron–ion pair created $\mathcal{E}^{(\alpha)}_\mathrm{c}$, given as [10]

$$\mathcal{E}^{(\alpha)}_\mathrm{c} = \mathcal{E}^{(\alpha)}_\mathrm{iz} + \sum_i \mathcal{E}^{(\alpha)}_{\mathrm{ex},i}\frac{k^{(\alpha)}_{\mathrm{ex},i}}{k^{(\alpha)}_\mathrm{iz}} + \frac{k^{(\alpha)}_\mathrm{el}}{k^{(\alpha)}_\mathrm{iz}}\frac{3m_\mathrm{e}}{m^{(\alpha)}}T_\mathrm{e} \qquad (15)$$

where $\mathcal{E}^{(\alpha)}_\mathrm{iz}$ is the ionization energy of species α, $\mathcal{E}^{(\alpha)}_{\mathrm{ex},i}$ is the energy for the ith excitation process of species α, $k^{(\alpha)}_{\mathrm{ex},i}$ is the rate coefficient for the ith excitation process of species α, $k^{(\alpha)}_\mathrm{el}$ is the elastic scattering rate coefficient of species α, m_e is the electron mass and $m^{(\alpha)}$ is the mass of species α. The ionization energies of the nitrogen atom and molecule are 14.5 eV and 15.6 eV, respectively [26]. The excitation energies of the various excited nitrogen atoms and molecules are taken from the NIST database [27] and from the review by Lofthus and Krupenie [28], respectively, and are not repeated here. The ionization, excitation and elastic scattering rate coefficients will be discussed in section 2.4.

2.3. The gas temperature

In the earlier global model calculations the gas temperature was commonly assumed to be 600 K and to be independent of the plasma parameters [15, 19], mainly because of lack of measurements thereof. However, for inductively coupled nitrogen discharges there exist several measurements of the gas temperature [29–35]. These measurements demonstrate that the gas temperature depends on the absorbed power but less on the discharge pressure. A linear least-squares fit to the measured data gives a gas temperature of $T_\mathrm{g} = 0.17 \times P_\mathrm{abs} + 387$ K, which we will assume applies to both ions and neutral nitrogen species. A more thorough discussion of the nitrogen gas temperature is given elsewhere [36].

2.4. The reaction set

The reaction set is summarized in tables 1–7. A detailed discussion of the reaction set and the cross sections used is given elsewhere [36]. The electron impact reactions that employ a cross section to calculate the rate coefficient are summarized in table 1. The cross sections for the dissociative excitation and dissociative ionization of the N_2^+ ion, reactions (R1) and (R2), given by Bahati *et al* [37], were multiplied by a factor of 3 in order to reach an agreement with other similar cross sections [38–40]. We have assumed that only one of the products of electron impact dissociation, reaction (R6), is atomic nitrogen in the ground state N(^{4}S), consistent with reports of two N(^{4}S) atoms almost never being formed in a single dissociation event [41, 42]. We assume that the cross sections for reactions (R3) to (R7) only apply to an $N_2(X\,^1\Sigma_\mathrm{g}^+, v = 0)$ reactant. We obtain cross sections for reactions with $N_2(X\,^1\Sigma_\mathrm{g}^+, v > 0)$ and $N_2(A\,^3\Sigma_\mathrm{u}^+)$ reactants by reducing the threshold of the cross sections [43] for the corresponding $N_2(X\,^1\Sigma_\mathrm{g}^+, v = 0)$ reaction according to the excitation energies of the reactants [28]. The magnitude of the cross section is kept the same, except for the electron impact ionization of $N_2(A\,^3\Sigma_\mathrm{u}^+)$, reactions (R3) to (R5), that are made 20% larger as indicated by the measurement of Freund *et al* [44]. These reactions, although certainly used in our model, are not shown in table 1. The reaction set for electron impact vibrational excitation of $N_2(X\,^1\Sigma_\mathrm{g}^+, v)$, reactions (R8) to (R11), is incomplete. Although transitions from the $v = 0$ state are relatively well documented, cross sections for transitions between higher vibrational levels are scarce [45–47] and, in the case of the chosen data, are not given for all possible transitions. To estimate the cross sections for the remaining vibrational level transitions we reduce the threshold of the appropriate cross sections calculated by Dubé and Herzenberg [46]. Since the maximum value of the cross sections clearly decreases with both increasing vibrational level and increasing jump size, we also scale the magnitude of each cross section according to a fit to a particular pattern thereof [36]. The resulting magnitude scaling factors, varying between 0.74 and 0.94, are not significant and are expected to have only a minor effect on the vibrational level population. Each of the electron impact excitation reactions has an inverse counterpart in the reaction set. These cross sections are

Table 1. Electron impact reactions that use cross sections instead of rate coefficients.

	Reaction	Reference
(R1)	$e + N_2^+ \rightarrow N(^2D) + N^+ + e$	[37][a]
(R2)	$e + N_2^+ \rightarrow N^+ + N^+ + 2e$	[37][a]
(R3)	$e + N_2(X\,^1\Sigma_g^+, v = 0) \rightarrow N_2^+ + 2e$	[66]
(R4)	$e + N_2(X\,^1\Sigma_g^+, v = 0) \rightarrow N(^2D) + N^+ + 2e$	[66]
(R5)	$e + N_2(X\,^1\Sigma_g^+, v = 0) \rightarrow N^+ + N^+ + 3e$	[66]
(R6)	$e + N_2(X\,^1\Sigma_g^+, v = 0) \rightarrow N(^4S) + N(^2D) + e$	[41]
(R7)	$e + N_2(X\,^1\Sigma_g^+, v = 0) \rightarrow N_2(A\,^3\Sigma_u^+) + e$	[50]
(R8)	$e + N_2(X\,^1\Sigma_g^+, v = 0) \rightarrow N_2(X\,^1\Sigma_g^+, v = 1\text{–}6) + e$	[67]
(R9)	$e + N_2(X\,^1\Sigma_g^+, v = 1) \rightarrow N_2(X\,^1\Sigma_g^+, v = 2\text{–}4) + e$	[46]
(R10)	$e + N_2(X\,^1\Sigma_g^+, v = 2) \rightarrow N_2(X\,^1\Sigma_g^+, v = 3\text{–}5) + e$	[46]
(R11)	$e + N_2(X\,^1\Sigma_g^+, v = 3) \rightarrow N_2(X\,^1\Sigma_g^+, v = 4\text{–}6) + e$	[46]
(R12)	$e + N(^4S, ^2D, ^2P) \rightarrow N^+ + 2e$	[68]
(R13)	$e + N(^4S, ^2D) \rightarrow N(^2D, ^2P) + e$	[59]
(R14)	$e + N_2(X\,^1\Sigma_g^+, v = 0) \rightarrow N_2(X\,^1\Sigma_g^+, v = 0) + e$	[49, 50][b,c]
(R15)	$e + N(^4S) \rightarrow N(^4S) + e$	[51, 52][b,c]
(R16)	$e + N(^4S) \rightarrow N([3s, 2s2p^4, 4s, 3d]\,^4P) + e$	[59][c]
(R17)	$e + N_2(X\,^1\Sigma_g^+, v = 0) \rightarrow N_2(B\,^3\Pi_g - a''\,^1\Sigma_g^+) + e$	[50][c]

[a] Magnitude of cross section multiplied by 3. See text.
[b] Cross section is a compilation. See text.
[c] Only used for the calculation of $\mathcal{E}_c$.

obtained by the principle of detailed balancing [48],

$$\sigma'(\mathcal{E}') = \left(1 + \frac{\mathcal{E}_a}{\mathcal{E}'}\right) \frac{g_r}{g_p} \sigma(\mathcal{E}' + \mathcal{E}_a), \tag{16}$$

where g_r and g_p are the degeneracies of the reactant and product, respectively, in the direct reaction and $\mathcal{E}_a$ is the reaction energy threshold.

The elastic scattering cross sections, reactions (R14) and (R15), are only used in the calculation of the collisional energy loss, $\mathcal{E}_c$, having no effect on the particle balance. The cross section for elastic scattering by $N_2(X\,^1\Sigma_g^+, v = 0)$, reaction (R14), is composed of two cross sections in the range 20 meV–3.5 eV [49] and 4–1000 eV [50]. The cross section for elastic scattering by $N(^4S)$, reaction (R15) is composed of two cross sections in the range 25 meV–3.5 eV [51] and 5–9 eV [52]. The collisional energy loss also consists of the electron impact excitation of the nitrogen atom and nitrogen molecule. In addition to reaction (R13) we consider the electron impact excitation of the $3s^4P$, $2s2p^4\ ^4P$, $4s^4P$ and $3d^4P$ levels of the nitrogen atom, i.e. reaction (R16). For the molecule, we consider the electron impact excitation of the $B\,^3\Pi_g$, $W\,^3\Delta_u$, $B'\,^3\Sigma_u^-$, $a''\,^1\Sigma_u^-$, $a\,^1\Pi_g$, $w\,^1\Delta_u$, $C\,^3\Pi_u$, $E\,^3\Sigma_g^+$ and $a''\,^1\Sigma_g^+$ electronic states of the nitrogen molecule, i.e. reaction (R17), in addition to reactions (R7) and (R8).

Reactions involving positive ions are given in table 2 along with their rate coefficients. Reactions where the state of a neutral reactant is unspecified are assumed to occur with equal probability for all electronic and vibrational levels of that neutral. Dissociative recombination, reactions (R18) to (R20), should be represented by a cross section instead of an electron energy distribution independent rate coefficient, but since no cross sections could be found that were given over a sufficiently wide electron energy range, a rate coefficient was used instead. The products of the dissociative recombination of N_2^+ branch to $[N(^2D) + N(^2D)] : [N(^4S) + N(^2D)] : [N(^4S) + N(^2P)]$ with the ratio 0.47 : 0.34 : 0.19 [38]. Since at least one of the products is believed to be in an excited state, we will assume that the products of dissociative recombination of N_3^+ branch to $[N_2(A\,^3\Sigma_u^+) + N(^4S)] : [N_2(X\,^1\Sigma_g^+, v = 0) + N(^2P)]$ with the ratio arbitrarily chosen as 0.5 : 0.5. Similarly, we will assume that the products in dissociative recombination of N_4^+ are always $N_2(A\,^3\Sigma_u^+)$ and $N_2(X\,^1\Sigma_g^+, v = 0)$. The associative ionization of two $N_2(A\,^3\Sigma_u^+)$, reaction (R22), is actually an endothermic reaction. However, in order to estimate an upper limit of the overall production of N_4^+ without having to include higher lying excited molecules we will assume that effectively the reaction occurs and has a rate coefficient that is equal to the rate coefficient of associative ionization of two $N_2(X\,^1\Sigma_g^+, v > 32)$ molecules. The resulting N_4^+ density should therefore only be considered as an upper limit. The charge transfer reaction (R26) is only exothermic when the reactant molecule has energy above the $N_2(X\,^1\Sigma_g^+, v = 3)$ level, and is therefore assumed not to occur when the reactant is in a state below $N_2(X\,^1\Sigma_g^+, v \leqslant 3)$.

A set of reactions where the electronic excitation of nitrogen atoms and molecules is quenched or transferred to the colliding particle is given in table 3. The rate coefficients for reactions (R30) to (R33) are assumed to apply to all vibrational and electronic states of the neutral molecule or atom whose state is unspecified. The reactions where the vibrational excitation of the ground state nitrogen molecule $N_2(X\,^1\Sigma_g^+, v)$ is quenched or transferred in a collision of two neutral nitrogen molecules are given in table 4. The rate coefficient for reaction $N_2(X\,^1\Sigma_g^+, v = 5 - 6) + N_2(A\,^3\Sigma_u^+)$ (R35) is assumed to be equal to the rate coefficient measured for pooling of energy in the collision of $N_2(A\,^3\Sigma_u^+)$ and $N_2(X\,^1\Sigma_g^+, v \geqslant 5)$, forming an $N_2(B\,^3\Pi_g)$ instead of $N_2(A\,^3\Sigma_u^+)$. Since the $N_2(B\,^3\Pi_g)$ is not metastable and radiates quickly back to $N_2(A\,^3\Sigma_u^+)$ with a lifetime of only a few microseconds [53] the assumption is likely satisfactory. Each of the rate coefficients for reactions

Table 2. Rate coefficients for reactions involving positive nitrogen ions.

	Reaction	Rate coefficient ($m^3\,s^{-1}$)	Reference
(R18)	$e + N_2^+ \rightarrow N + N$	$1.90 \times 10^{-15} T_e^{-0.30}$	[38]
(R19)	$e + N_3^+ \rightarrow N_2 + N$	$3.22 \times 10^{-14} T_e^{-0.50}$	[69]
(R20)	$e + N_4^+ \rightarrow N_2 + N_2$	$3.20 \times 10^{-13} T_e^{-0.50}$	[69]
(R21)	$N(^2D, ^2P) + N(^2P) \rightarrow N_2^+ + e$	1.00×10^{-18}	[69]
(R22)	$2N_2(A\,^3\Sigma_u^+) \rightarrow N_4^+ + e$	1.00×10^{-19}	[70][a]
(R23)	$N_2(A\,^3\Sigma_u^+) + N_2^+ \rightarrow N(^4S) + N_3^+$	5.50×10^{-17}	[71]
(R24)	$N + N_3^+ \rightarrow N_2(A\,^3\Sigma_u^+) + N_2^+$	6.60×10^{-17}	[69]
(R25)	$N + N_2^+ \rightarrow N_2 + N^+$	$7.20 \times 10^{-19} (300/T_g)^{-1}$	[69]
(R26)	$N_2(X\,^1\Sigma_g^+, v = 4\text{–}6) + N^+ \rightarrow N(^4S) + N_2^+$	2.00×10^{-17}	[3]
(R27)	$N_2(A\,^3\Sigma_u^+) + N^+ \rightarrow N(^2P) + N_2^+$	2.00×10^{-17}	[3]
(R28)	$N + N_4^+ \rightarrow N_2 + N_2 + N^+$	1.00×10^{-17}	[69]
(R29)	$N_2 + N_4^+ \rightarrow N_2 + N_2 + N_2^+$	$8.67 \times 10^{-23} (300/T_g)^{-6.45} \exp(900/T_g)$	[70, 72]

[a] Rate coefficient estimated to be equal to a similar reaction.

Table 3. Reactions involving quenching or transfer of electronic excitation of neutral nitrogen atoms and molecules.

	Reaction	Rate coefficient ($m^3\,s^{-1}$)	Reference
(R30)	$N_2 + N_2(A\,^3\Sigma_u^+) \rightarrow N_2 + N_2(X\,^1\Sigma_g^+, v = 0)$	3.00×10^{-24}	[69, 73]
(R31)	$N_2 + N(^2D) \rightarrow N_2 + N(^4S)$	1.30×10^{-20}	[74]
(R32)	$N_2 + N(^2P) \rightarrow N_2 + N(^4S)$	3.30×10^{-23}	[74]
(R33)	$N + N(^2P) \rightarrow N + N(^4S)$	6.20×10^{-19}	[75]
(R34)	$N_2(A\,^3\Sigma_u^+) + N(^4S) \rightarrow N_2(X\,^1\Sigma_g^+, v = 0) + N(^2P)$	4.00×10^{-17}	[76]

Table 4. Reactions involving quenching or transfer of vibrational excitation of the ground state nitrogen molecule $N_2(X\,^1\Sigma_g^+, v = 1\text{–}6)$.

	Reaction	Rate coefficient ($m^3\,s^{-1}$)	Reference
(R35)	$N_2(v = 5-6) + N_2(A\,^3\Sigma_u^+) \rightarrow N_2(v = 0) + N_2(A\,^3\Sigma_u^+)$	3.00×10^{-17}	[77][a]
(R36)	$N_2(v = 1) + N_2 \rightarrow N_2(v = 0) + N_2$	$5.19 \times 10^{-28} (300/T_g)^{-8.51}$	[78]
(R37)	$N_2(v = 2) + N_2 \rightarrow N_2(v = 1) + N_2$	$1.15 \times 10^{-27} (300/T_g)^{-8.54}$	[78]
(R38)	$N_2(v = 3) + N_2 \rightarrow N_2(v = 2) + N_2$	$2.18 \times 10^{-27} (300/T_g)^{-8.53}$	[78]
(R39)	$N_2(v = 4) + N_2 \rightarrow N_2(v = 3) + N_2$	$4.32 \times 10^{-27} (300/T_g)^{-8.30}$	[78]
(R40)	$N_2(v = 5) + N_2 \rightarrow N_2(v = 4) + N_2$	$6.87 \times 10^{-27} (300/T_g)^{-8.27}$	[78]
(R41)	$N_2(v = 6) + N_2 \rightarrow N_2(v = 5) + N_2$	$1.10 \times 10^{-26} (300/T_g)^{-8.15}$	[78]
(R42)	$N_2(v = 1) + N_2(v = 1) \rightarrow N_2(v = 0) + N_2(v = 2)$	$1.73 \times 10^{-20} (300/T_g)^{-1.42}$	[78]
(R43)	$N_2(v = 1) + N_2(v = 2) \rightarrow N_2(v = 0) + N_2(v = 3)$	$2.18 \times 10^{-20} (300/T_g)^{-1.54}$	[78]
(R44)	$N_2(v = 1) + N_2(v = 3) \rightarrow N_2(v = 0) + N_2(v = 4)$	$2.60 \times 10^{-20} (300/T_g)^{-1.55}$	[78]
(R45)	$N_2(v = 1) + N_2(v = 4) \rightarrow N_2(v = 0) + N_2(v = 5)$	$2.80 \times 10^{-20} (300/T_g)^{-1.63}$	[78]
(R46)	$N_2(v = 1) + N_2(v = 5) \rightarrow N_2(v = 0) + N_2(v = 6)$	$3.09 \times 10^{-20} (300/T_g)^{-1.63}$	[78]

[a] The rate coefficient is for a reaction with the product molecule in a higher level than the $N_2(A\,^3\Sigma_u^+)$.

(R36) to (R41) are assumed to apply to all vibrational states of the neutral molecule whose state is unspecified. The transfer of vibrational excitation,

$$N_2(v = j) + N_2(v = k) \rightarrow N_2(v = j + 1) + N_2(v = k - 1) \tag{17}$$

is given for $k = 1$ in reactions (R42) to (R46). The rest of the reactions with $k > 1$ are derived from the rate coefficient in table 4 for $k = 1$ and $j = j'$ by [54, 55]

$$K_{k,k-1}^{j,j+1} = \frac{k(j+1)}{j'+1} K_{1,0}^{j',j'+1} \tag{18}$$

when $j' = k - j - 1$. When $j' = j + 1 - k$, the reaction is slightly endothermic and the right hand side of equation (18) must be multiplied by $\exp(-\Delta E/kT)$, where $\Delta E = E_k + E_j - E_{k-1} - E_{j+1}$ is the vibrational energy defect.

The set of reactions involving association of two particles in an interaction of three particles (three body reactions) is given in table 5. Each rate coefficient is assumed to apply to all combinations of electronic and vibrational levels of the reactants. Reactions representing the radiative decay of excited species are given in table 6. Since the ground state nitrogen molecule has no permanent dipole moment, electric dipole radiation from $N_2(X\,^1\Sigma_g^+, v = 1 - 6)$ to $N_2(X\,^1\Sigma_g^+, v = 0)$ is not permitted and is assumed not to occur.

2.5. Losses to walls

The diffusional losses of the neutral nitrogen species to the reactor walls are estimated by an effective loss-rate coefficient, given by [56]

$$k_{n,\text{wall}} = \left[\frac{\Lambda_n^2}{D_n} + \frac{2V(2 - \gamma_n)}{A \bar{v}_n \gamma_n} \right]^{-1}, \tag{19}$$

Table 5. Reactions involving the interaction of three gas particles.

	Reaction	Rate coefficient ($m^6\,s^{-1}$)	Reference
(R47)	$N_2 + N + N \rightarrow N_2 + N_2$	$8.27 \times 10^{-46} \exp(500/T_g)$	[69, 70]
(R48)	$N + N + N \rightarrow N_2 + N$	1.00×10^{-44}	[70]
(R49)	$N_2 + N + N^+ \rightarrow N_2 + N_2^+$	1.00×10^{-41}	[69]
(R50)	$N_2 + N_2 + N_2^+ \rightarrow N_2 + N_4^+$	$5.20 \times 10^{-41} (300/T_g)^{2.20}$	[79]
(R51)	$N_2 + N_2 + N^+ \rightarrow N_2 + N_3^+$	$1.70 \times 10^{-41} (300/T_g)^{2.10}$	[79]
(R52)	$N_2 + N + N_2^+ \rightarrow N_2 + N_3^+$	$9.00 \times 10^{-42} \exp(400/T_g)$	[69]

Table 6. The reaction set for optical emission of excited species.

	Reaction	Rate coefficient (s^{-1})	Reference
(R53)	$N_2(A\,^3\Sigma_u^+) \rightarrow N_2(X\,^1\Sigma_g^+, v = 0) + \hbar\omega$	4.22×10^{-1}	[80]
(R54)	$N(^2P) \rightarrow N(^4S) + \hbar\omega$	5.40×10^{-3}	[81]
(R55)	$N(^2P) \rightarrow N(^2D) + \hbar\omega$	5.30×10^{-2}	[82]
(R56)	$N(^2D) \rightarrow N(^4S) + \hbar\omega$	1.90×10^{-5}	[82]

where D_n is the neutral diffusion coefficient given by [48]

$$D_n = \frac{eT_g\lambda_n}{\bar{v}_n m_n} \tag{20}$$

and $\bar{v}_n = (8eT_g/\pi m_n)^{1/2}$ is the mean neutral velocity, γ_n is the sticking coefficient for the neutral particle on the wall surface, m_n is the neutral mass and V and A are the volume and the wall surface area of the reactor chamber, respectively, and λ_n is the mean free path of the neutral particle, given by

$$\frac{1}{\lambda} = \sum_j n_j \sigma_{sc_j} \tag{21}$$

where n_j is the density of the gas species j and σ_{sc_j} is the scattering cross section for the collision with the gas species j. The sum of the charge exchange and momentum transfer cross sections given by Phelps [57] is used as a basis for our scattering cross sections. We extrapolated a value for the cross sections at 0.05 eV [48, p 80], yielding about 50 Å^2 for N_2–N_2 collisions, 250 Å^2 for N_2–N_2^+ collisions, and 150 Å^2 for N_2–N^+ collisions. The cross sections for other collisions were derived by assuming that the scattering cross section is proportional to the combined number of atoms in the collisions, as indicated by the hard sphere model. All ion–ion scattering cross sections were assumed to be zero. The effective diffusion length of each of the neutral species is given by [58]

$$\Lambda_n = \left[\left(\frac{\pi}{L}\right)^2 + \left(\frac{2.405}{R}\right)^2 \right]^{-1/2}. \tag{22}$$

The ion flux to the walls is assumed to have the rate coefficient

$$k_{+,\text{wall}} = 2u_B \frac{R^2 h_L + RLh_R}{R^2 L}\ \text{s}^{-1}, \tag{23}$$

where u_B is the Bohm velocity, given by equation (6), m_i is the ion mass and h_L and h_R are the edge to center positive ion density ratios given as [12]

$$h_L \simeq 0.86 \left[3 + \frac{L}{2\lambda_i} + \left(\frac{0.86 L u_B}{\pi D_a} \right)^2 \right]^{-1/2} \tag{24}$$

and

$$h_R \simeq 0.80 \left[4 + \frac{R}{\lambda_i} + \left(\frac{0.80 R u_B}{\chi_{01} J_1(\chi_{01}) D_a} \right)^2 \right]^{-1/2}, \tag{25}$$

respectively, where $J_1(\chi)$ is the first order Bessel function, $\chi_{01} \simeq 2.405$ is the first zero of the zero order Bessel function J_0, $D_a = D_i(1 + \gamma)$ is the ambipolar diffusion coefficient, D_i is the diffusion coefficient (20) for positive ions, $\gamma = T_e/T_i$ is the fraction of the electron and ion temperatures and λ_i is the mean free path of ions. The third term in the expressions for the scaling factors was added in this work and was not included in our previous model of the O_2/Ar discharge [19] to account for diffusion at higher pressures, approximately in the range 30–100 mTorr. This addition is expected to decrease the effective area for ion loss,

$$A_{\text{eff}} = 2\pi(R^2 h_L + RLh_R), \tag{26}$$

compared with previous models since the scaling factors, h_L and h_R, decrease. The interactions of neutrals and ions with the wall are summarized in table 7.

2.6. Pumping losses

The rate due to the flow of a certain gas species into a chamber of volume V is given by $R = 4.48 \times 10^{17} Q_{in}/V$, where Q_{in} is the flow of the species into the chamber in sccm and the scalar converts sccm to particles s^{-1}. Similarly, the rate due to the flow of gas out of the chamber is given by $R = 1.27 \times 10^{-5} n Q_{in}/pV$, where n is the density of the species being pumped out, Q_{in} is the total flow of gas into the chamber in sccm, p is the outlet-flow pressure in Torr and the scalar converts sccm to Torr m^3 s^{-1}.

3. Results and discussion

We apply a global (volume averaged) model in the steady state to study the nitrogen discharge. We explore the dependence of the plasma parameters on the discharge pressure, absorbed power and the electron energy distribution function. The

Table 7. The interaction of positive ions and neutral nitrogen atoms and molecules with the reactor walls.

	Reaction	Rate coefficient (s^{-1})	γ_n
(R57)	$N(^4S,^2D,^2P) + \text{wall} \rightarrow \frac{1}{2}N_2(X\,^1\Sigma_g^+, v=0)$	$\left[\frac{\Lambda_0^2}{D_N} + \frac{2V(2-\gamma_n)}{A\bar{v}_N\gamma_n}\right]^{-1}$	0.07 [83]
(R58)	$N_2(X\,^1\Sigma_g^+, v) + \text{wall} \rightarrow N_2(X\,^1\Sigma_g^+, v-1)$	$\left[\frac{\Lambda_0^2}{D_{N_2(v)}} + \frac{2V(2-\gamma_n)}{A\bar{v}_{N_2(v)}\gamma_n}\right]^{-1}$	1.0
(R59)	$N_2(A\,^3\Sigma_u^+) + \text{wall} \rightarrow N_2(X\,^1\Sigma_g^+, v=0)$	$\left[\frac{\Lambda_0^2}{D_{N_2^*}} + \frac{2V(2-\gamma_n)}{A\bar{v}_{N_2^*}\gamma_n}\right]^{-1}$	1.0 [84]
(R60)	$N(^2D,^2P) + \text{wall} \rightarrow N(^4S)$	$\left[\frac{\Lambda_0^2}{D_{N^*}} + \frac{2V(2-\gamma_n)}{A\bar{v}_{N^*}\gamma_n}\right]^{-1}$	0.93[a]
(R61)	$N^+ + \text{wall} \rightarrow N(^4S)$	$2u_{B,N^+}(R^2h_L + RLh_R)/R^2L$	
(R62)	$N_2^+ + \text{wall} \rightarrow N_2(X\,^1\Sigma_g^+, v=0)$	$2u_{B,N_2^+}(R^2h_L + RLh_R)/R^2L$	
(R63)	$N_3^+ + \text{wall} \rightarrow N_2(X\,^1\Sigma_g^+, v=0) + N(^4S)$	$2u_{B,N_3^+}(R^2h_L + RLh_R)/R^2L$	
(R64)	$N_4^+ + \text{wall} \rightarrow N_2(X\,^1\Sigma_g^+, v=0) + N_2(X\,^1\Sigma_g^+, v=0)$	$2u_{B,N_4^+}(R^2h_L + RLh_R)/R^2L$	

[a] Value assumed to be equal to $1 - \gamma_{rec}$.

mechanism of dissociation will be considered, in particular, by evaluating the relative reaction rates of the creation and dissociation of atoms and the atomic ion N^+.

3.1. The collisional energy loss

The collisional energy loss per electron–ion pair created represents the power loss due to elastic and inelastic collisions and is an essential part of the power balance equation (14). The collisional loss $\mathcal{E}_c^{(N_2)}$, the energy loss per electron–N_2^+ pair created and $\mathcal{E}_c^{(N)}$, the energy loss per electron–N^+ pair created, have been calculated using rate coefficients generated from the relevant cross sections given in table 1 and the relevant cross sections for the electron impact excitation to higher electronic levels of nitrogen atoms [59] and molecules [50]. The result is shown in figure 1(*a*) for a Maxwellian-like electron energy distribution function. The collisional energy losses are very similar for the two species when the electron temperature is above 3 V, the collisional loss of the molecule increasing significantly faster when the electron temperature decreases any further. The collisional loss for the molecule is about 1400 and about 870 V for the atom when the electron temperature is 2.5 V, but have a very similar value at 100 V, or roughly 16 V and 18.8 V, respectively. Figure 1(*b*) shows the collisional loss of the molecular and atomic nitrogen calculated assuming a Druyvesteyn electron energy distribution. The collisional energy losses are very similar for the two species when the electron temperature is high, but unlike in the case of the Maxwellian electron energy distribution, the collisional losses become different much sooner, or when the electron temperature is below roughly 7 V, and increase substantially more rapidly with decreasing electron temperature. The collisional loss is now approximately 2×10^7 V for the molecule and about 4×10^5 V for the atom when the electron temperature is 2.5 V, much larger than for the Maxwellian electron energy distribution. When the electron temperature is 100 V the collisional losses are very similar, or 15.8 V and 16.8 V for the molecule and atom, respectively.

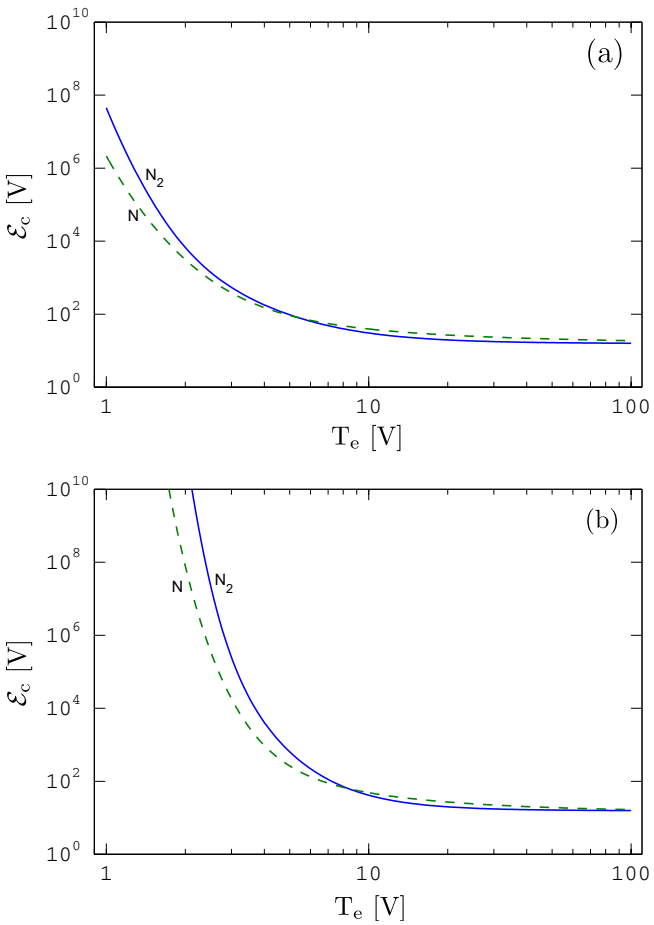

Figure 1. The collisional energy loss per electron–ion pair created, $\mathcal{E}_c$, as a function of the electron temperature for the ground state nitrogen molecule, $N_2(X\,^1\Sigma_g^+, v=0)$, and the ground state nitrogen atom, $N(^4S)$, when assuming (*a*) a Maxwellian electron energy distribution and (*b*) a Druyvesteyn electron energy distribution.

3.2. Comparison with measurements

In figures 2 to 4 we compare the model calculations for a Maxwellian electron energy distribution function with

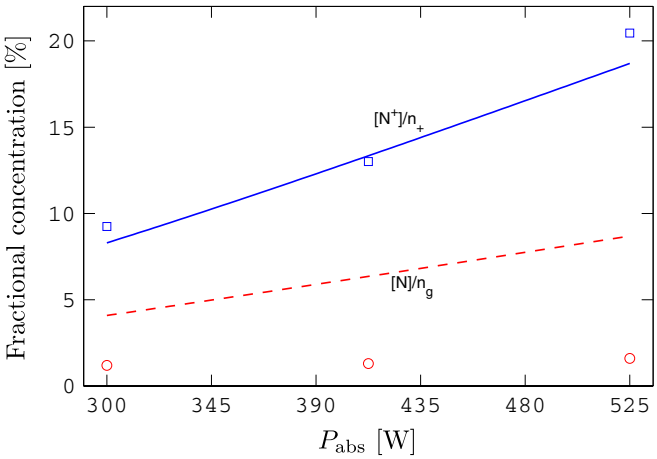

Figure 2. Comparison of the model calculations (lines) with the atomic ion fraction $[N^+]/n_+$ (○) and the dissociation fraction $[N]/n_g$ (□) measured by Singh and Graves [22] as a function of the applied power ($P_{abs} \simeq 0.75 \times P_{rf}$) in a stainless steel chamber with $R = 10$ cm and $L = 10$ cm. The discharge pressure was maintained at 30 mTorr and the gas flowrate was assumed to be 50 sccm.

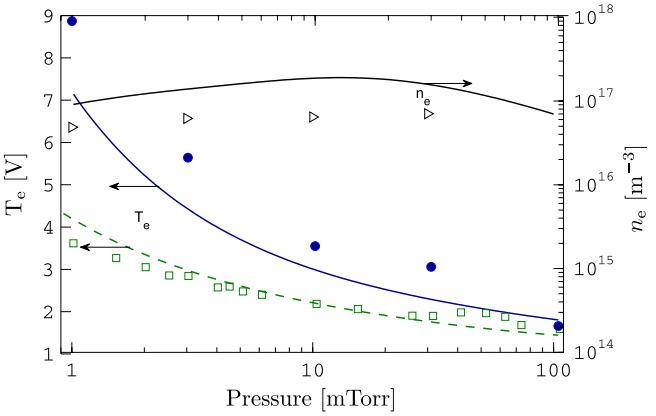

Figure 3. Model calculations (——) compared with the electron temperature (●) and electron density (▷) measured by Singh and Graves [21] in a stainless steel chamber with the dimensions $R = 10$ cm and $L = 10$ cm and an absorbed power of 320 W. Also shown is a comparison of the calculated electron temperature (----) with the measurement by Zhu and Pu [62] (□) in a stainless steel chamber with $R = 30$ cm and $L = 40$ cm and a total power of 600 W applied to the discharge ($P_{abs} \simeq 450$ W). The gas flowrate was assumed to be 50 sccm for both cases.

measurements found in the literature. Singh and Graves [22] measured the fractional dissociation and the fractional density of ions versus the discharge power in an inductively coupled discharge in a stainless steel chamber with the dimensions $R = 10$ cm and $L = 10$ cm. The gas flow rate into the chamber was not specified and we will therefore assume a 50 sccm gas flow rate in the calculation. Since only the total rf-power was specified for the measurement, we will assume a 75% power coupling efficiency, i.e. $P_{abs}/P_{rf} = 0.75$ [60]. The authors claim the power deposition efficiency to be in the range 50–80% in their experimental setup [61]. The measured dissociation fraction, $[N]/n_g$, and the measured ratio of the N^+ ion versus the total ion density, $[N^+]/n_+$, are compared with our model calculations in figure 2. The measured fraction of the N^+ ion is in excellent agreement with our calculations while the dissociation fraction is about a factor of 3–5 larger in our calculation than the measurement. Since the fraction of atomic ions is about a factor of 7–13 larger than the fraction of atomic neutrals, we believe it is unlikely that both the measurements are accurate. By scaling down the cross section for electron impact dissociation, reaction (R6), by a factor of 5 we got the same level of dissociation as in the measurement, but then there was a poor agreement with the measured N^+ fraction. Thus, if both the measurements were to be accurate, the seemingly reliable cross section for electron impact ionization of N, reaction (R12), would need to be made substantially larger in addition to the modified dissociation cross section. The large dissociation fraction might also be explained by the cross sections for the dissociation of vibrationally excited molecules being significantly smaller than for $N_2(X\,^1\Sigma_g^+, v = 0)$, instead of having the same magnitude as we have assumed in this study. In fact, excluding the $N_2(X\,^1\Sigma_g^+, v = 1\text{–}6)$ in the model calculations entirely has a similar effect as decreasing the dissociation cross section by a factor of 5, the N^+ fraction being in poor agreement with the measurement while the dissociation fraction is spot-on.

Singh and Graves [21] also measured the electron temperature and the electron density versus the discharge pressure in the same chamber. The reported absorbed power was 320 W, but since the gas flowrate was not specified we assumed a value of 50 sccm for the calculations. The measured electron density and electron temperature are compared with our model calculations in figure 3. The calculations are in good agreement with the measurements. The electron density is at most roughly a factor of 3 larger than the measured values, which is actually worse than the agreement of our model with other electron density measurements [9, 62]. The calculated electron temperature, although being somewhat too low, exhibits the same behavior with pressure as observed in the measurement. Also shown in figure 3 is the electron temperature measured by Zhu and Pu [62] by optical emission spectroscopy instead of the usual Langmuir probe method. The inductively coupled discharge chamber was cylindrical with the dimensions $R = 30$ cm and $L = 40$ cm. The applied power was 600 W, corresponding to $P_{abs} = 450$ W assuming the power coupling efficiency is 75% as before. The gas flowrate was assumed to be 50 sccm, as it was not specified for the measurement. The measured electron temperature is in excellent agreement with our calculations.

Agarwal *et al* [63] measured the atomic density and the metastable molecule density versus the discharge pressure by optical emission spectroscopy. The stainless steel chamber was cylindrical with the dimensions $R = 15$ cm and $L = 18$ cm [64]. The applied power was 750 W (absorbed power 563 W in the calculation) and the gas flowrate was 50 sccm. The measurements are compared with our model calculations in figure 4. The calculated $N_2(A\,^3\Sigma_u^+)$ density is in good agreement with the measured values, being somewhat larger. However, the atomic density is in much worse agreement with the measurement, especially at low pressure, the difference being consistent with the dissociation fraction discrepancy shown in figure 2. This indicates that the

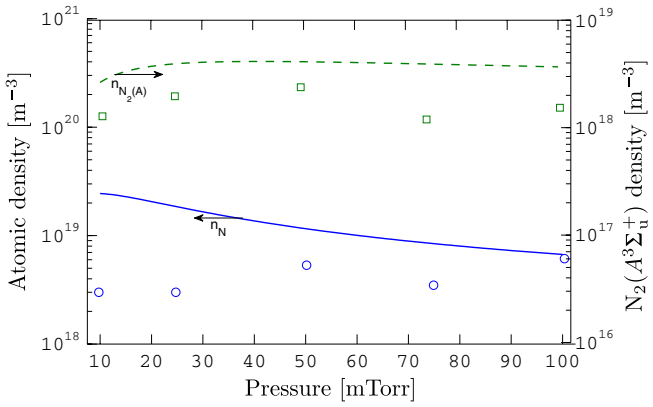

Figure 4. Comparison of the model calculations (lines) with the atomic density (○) and the $N_2(A\,^3\Sigma_u^+)$ density (□) measured by Agarwal *et al* [63] in a stainless steel chamber with $R = 15$ cm and $L = 18$ cm. The total applied power was 750 W ($P_{abs} \simeq 563$ W) and the gas flowrate was 50 sccm.

dissociation fraction is indeed overestimated by our model. However, it is not always the case since a comparison of our model calculations with the measurements of Biloiu *et al* [34] reveals a perfect agreement, or 13% dissociation fraction at the given conditions ($R = 15$ cm, $L = 30$ cm, $P_{rf} = 500$ W, $P_{abs} = 375$ W, $p = 10$ mTorr and $Q = 50$ sccm). Other studies have demonstrated that different methods, such as optical and mass spectroscopic methods, yield vastly different dissociation fractions [1, 65]. Thus, we believe that our atomic density calculations are no more questionable than the atomic density or dissociation fraction measurements.

3.3. Dependence on pressure

The density of neutral nitrogen species versus the discharge pressure is shown in figure 5(*a*). The absorbed power is 500 W and the gas flowrate is 50 sccm. The chamber is assumed to be made of stainless steel, cylindrical with the dimensions $R = 10$ cm and $L = 10$ cm. The electron energy distribution function is assumed to be Maxwellian-like. The density of $N_2(X\,^1\Sigma_g^+, v = 0)$ increases almost linearly with pressure as the atomic density peaks at intermediate pressure. The vibrationally excited ground state molecules are a negligible part of the overall molecular density at low pressures, but increase such that at 100 mTorr the $N_2(X\,^1\Sigma_g^+, v = 1)$ density is comparable to the $N_2(X\,^1\Sigma_g^+, v = 0)$ density and the $N_2(X\,^1\Sigma_g^+, v = 6)$ is only a factor of 3 lower. The density of the metastable atoms is similarly closer to the ground state atom density at higher pressure, but are negligible at low pressure. The density of $N_2(A\,^3\Sigma_u^+)$ increases with pressure, but is at least two orders of magnitude lower than the $N_2(X\,^1\Sigma_g^+, v = 0)$ density. The density of electrons and the ions N^+, N_2^+, N_3^+ and N_4^+ is shown in figure 5(*b*). The electron density is relatively constant with pressure, but peaks at roughly 10–15 mTorr. The N_2^+ is the dominating ion at intermediate and high pressures, but is comparable to the N^+ density at lower pressure, although slightly larger. The density of the N^+ ion decreases so rapidly with pressure that the N_3^+ ion has a larger density above 70 mTorr. At 100 mTorr the N_3^+ ion represents roughly 10%

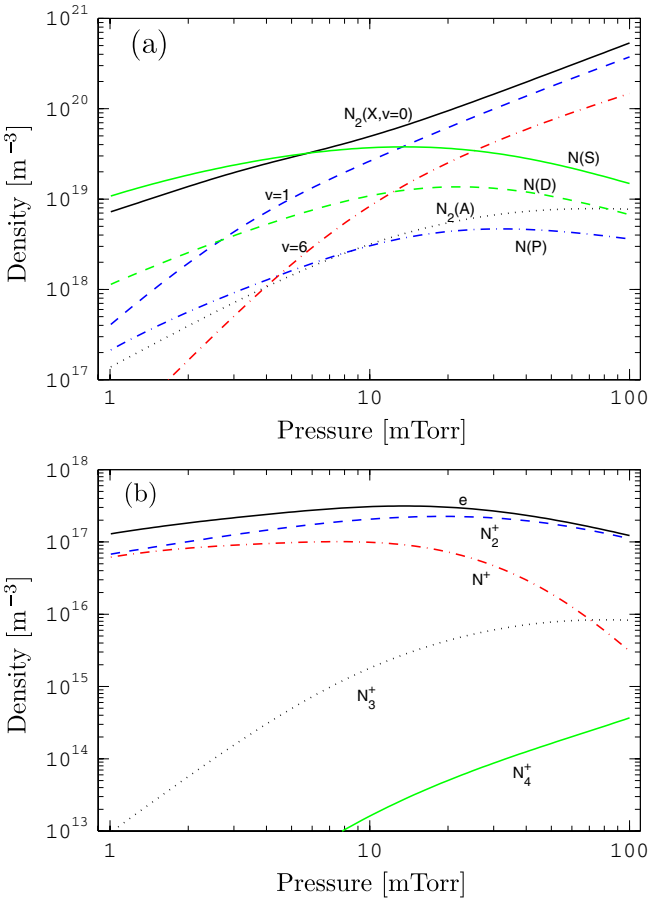

Figure 5. (*a*) The density of neutral nitrogen atoms and molecules and (*b*) the density of charged particles versus discharge pressure. The absorbed power is 500 W and the gas flowrate is 50 sccm. The chamber is assumed to be made of stainless steel, cylindrical with the dimensions $R = 10$ cm and $L = 10$ cm. The electron energy distribution function is assumed to be Maxwellian-like.

of the total ion density. The density of the N_4^+ ion increases rapidly with pressure as well, but is still an insignificant part of the total ion density at 100 mTorr.

The electron temperature versus pressure is shown in figure 6 for various absorbed powers under the same conditions as before. A well known characteristic of discharges is the weak dependence of the electron temperature with the absorbed power. This is the case for intermediate and high pressures, but at pressures below 10 mTorr the electron temperature becomes much more dependent on the absorbed power. For example, at 1 mTorr the electron temperature increases from about 7 to 11 V when the power is increased from 200 to 2000 W, whereas at 100 mTorr the electron temperature increases insignificantly with increased power.

The dissociation fraction $[N]/n_g$ is shown in figure 7 versus the discharge pressure for several absorbed powers under the same conditions as before. The dissociation fraction is heavily affected by both the discharge pressure and the absorbed power, being inversely dependent on the pressure and directly dependent on the power. At 100 mTorr the dissociation fraction is always low, not even being above 10% at a power of 2000 W. The situation is reversed at 1 mTorr, the dissociation fraction being about 35–85%, depending on the absorbed power.

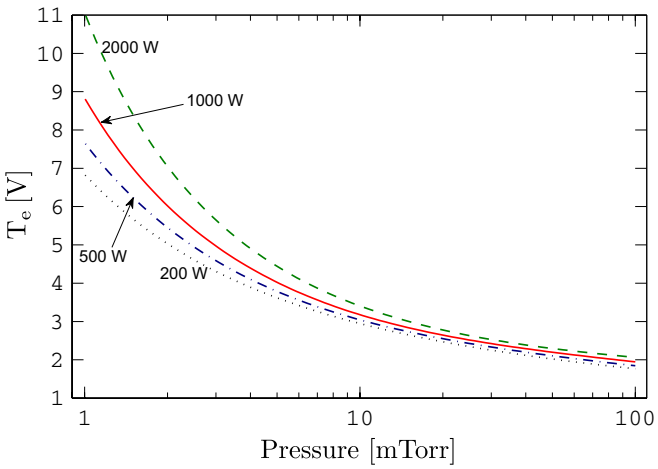

Figure 6. The electron temperature versus the discharge pressure for $P_{abs} = 200$, 500, 1000 and 2000 W. Conditions are as in figure 5.

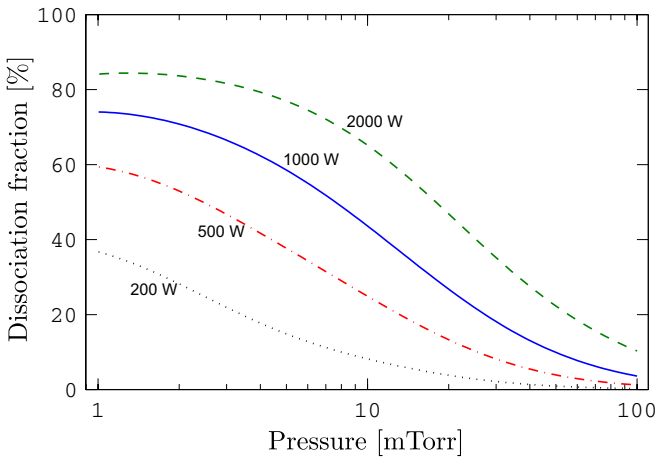

Figure 7. The dissociation fraction versus the discharge pressure for $P_{abs} = 200$, 500, 1000 and 2000 W. Conditions are as in figure 5.

The fraction of the N^+ ion versus the discharge pressure is shown in figure 8 for various absorbed powers under the same conditions as before. The N^+ fraction behaves similarly to the dissociation fraction, but has a less pronounced dependence on pressure and a slightly stronger dependence on the absorbed power. At 2000 W absorbed power the N^+ fraction peaks at about 4 mTorr, decreasing slightly when the pressure is decreased further.

The relative reaction rates for the overall creation and the overall destruction of the neutral nitrogen atom is shown in figures 9(*a*) and (*b*), respectively, as a function of the discharge pressure. Neutral nitrogen atoms are mostly created by electron impact dissociation, reaction (R6), over the entire pressure range, dissociation of $N_2(X\,^1\Sigma_g^+, v > 0)$ dominating at intermediate and high pressures. The contribution of dissociation of $N_2(X\,^1\Sigma_g^+, v = 0)$ is roughly 53% at 1 mTorr, but decreases and is less than 20% at 100 mTorr. Wall recombination of N^+, reaction (R61), is very important at low pressure, having a contribution of roughly 35% at 1 mTorr, but is negligible at high pressure. Neutral nitrogen atoms are lost mainly to wall recombination, reaction (R57), as is shown in figure 9(*b*). Pumping of $N(^4S)$ out of the chamber and electron

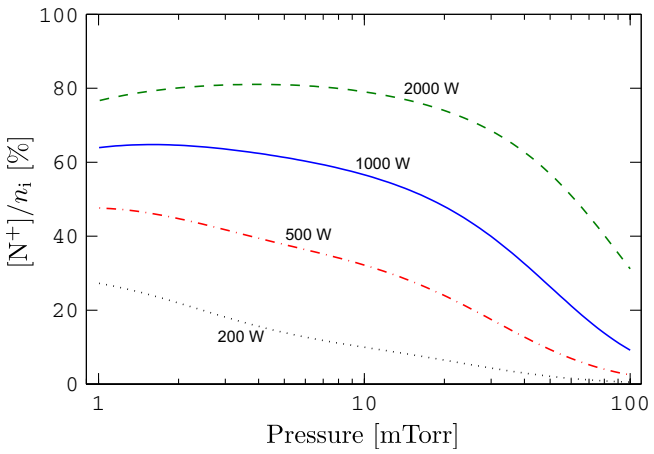

Figure 8. The fraction of the N^+ ion of the total ion density versus the discharge pressure for $P_{abs} = 200$, 500, 1000 and 2000 W. Conditions are as in figure 5.

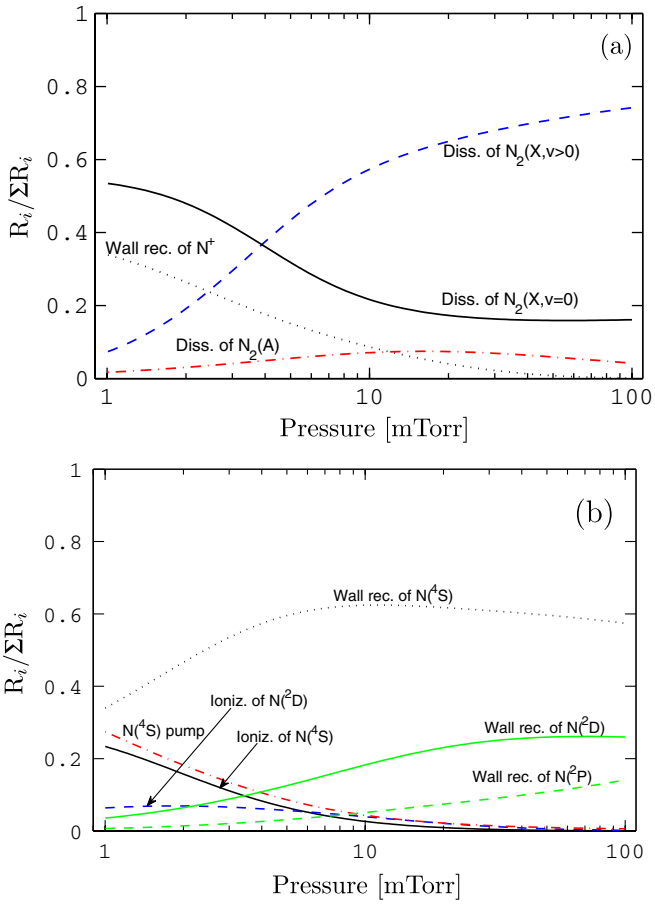

Figure 9. The relative reaction rates for (*a*) the overall creation and (*b*) the overall destruction of neutral nitrogen atoms. Conditions are as in figure 5.

impact ionization, reaction (R12), are significant loss processes at low pressure, each having a contribution of roughly 25–30% at 1 mTorr.

The reaction rates for the creation and destruction of N^+ are shown in figures 10(*a*) and (*b*), respectively, as a function of the discharge pressure under the same conditions as before. The atomic ion N^+ is mostly formed by electron impact ionization

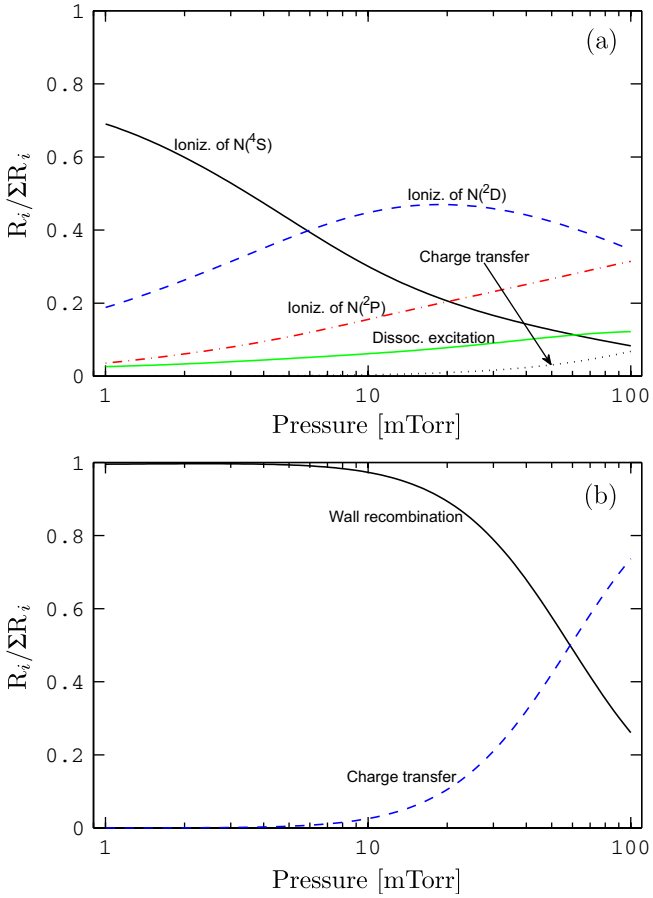

Figure 10. The relative reaction rates for (*a*) the creation and (*b*) the destruction of the N^+ ion. Conditions are as in figure 5.

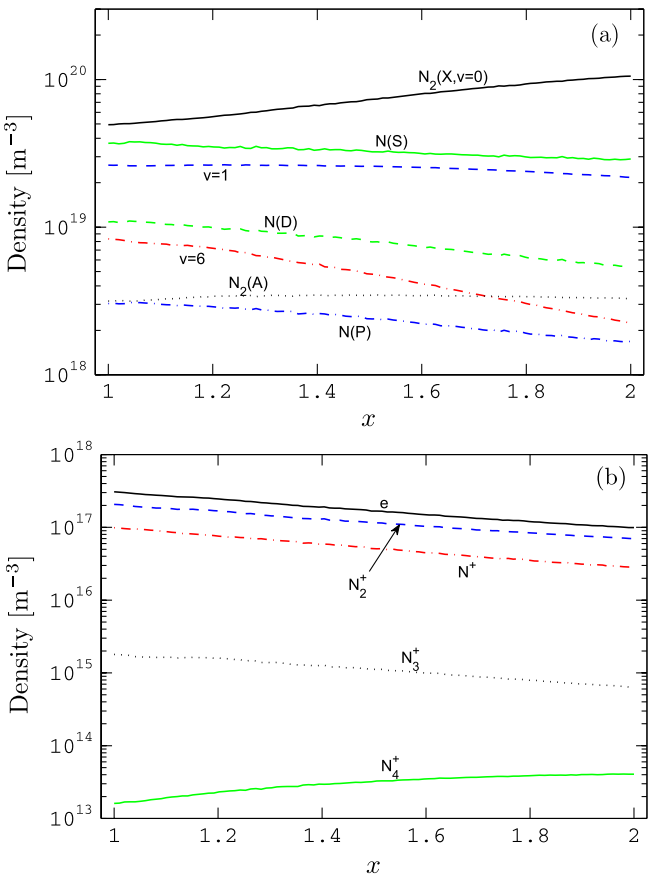

Figure 11. (*a*) The density of neutral nitrogen atoms and molecules and (*b*) the density of charged particles versus the electron energy distribution function. The absorbed power is 500 W, the discharge pressure 10 mTorr and the gas flowrate 50 sccm. The chamber is assumed to be made of stainless steel, cylindrical with the dimensions $R = 10$ cm and $L = 10$ cm.

of its neutral counterpart. The ionization of the ground state atom dominates at low pressure while ionization of metastable atoms is more important at high and intermediate pressures. Electron impact dissociative excitation of N_2^+, reaction (R1), has a significant contribution, increasing from roughly 3% at 1 mTorr to 12% at 100 mTorr. Charge transfer, reaction (R25), is only noticeable at high pressure with a 7% contribution at its maximum. As seen in figure 10(*b*), wall recombination is the dominating loss mechanism of the atomic ion N^+ at low and intermediate pressure, having a contribution of roughly 95–100% at 10–100 mTorr. However, charge transfer, reaction (R26), is very important at high pressure, being responsible for roughly 75% of the total N^+ loss at 100 mTorr.

3.4. Dependence on the electron energy distribution function

The density of neutral nitrogen species versus the electron energy distribution parameter x is shown in figure 11(*a*). The absorbed power is 500 W, the discharge pressure 10 mTorr and the gas flowrate 50 sccm. The chamber is assumed to be made of stainless steel, cylindrical with the dimensions $R = 10$ cm and $L = 10$ cm. The neutral densities are not as significantly affected by the electron energy distribution function as one might expect. In fact, the $N_2(A\,^3\Sigma_u^+)$ density is almost independent of x. The densities of $N_2(X\,^1\Sigma_g^+, v = 1)$ and $N(^4S)$ decrease only slightly when the distribution function is varied from being Maxwellian to Druyvesteyn-like by varying the parameter x in equation (1). The densities of $N(^2D)$ and $N(^2P)$ decrease by roughly a factor of 2. The most significant decrease is in the density of $N_2(X\,^1\Sigma_g^+, v = 6)$ which decreases by roughly a factor of 4. The densities of the other vibrational levels that are not shown, $N_2(X\,^1\Sigma_g^+, v = 2 - 5)$, are almost equally spaced between the $N_2(X\,^1\Sigma_g^+, v = 1)$ and $N_2(X\,^1\Sigma_g^+, v = 6)$ densities with increasing x. All of the density decreases seem to accumulate in the $N_2(X\,^1\Sigma_g^+, v = 0)$, its density increasing considerably with increasing x, or roughly by a factor of 2. The electron density, shown in figure 11(*b*), decreases significantly with varying electron energy distribution function, being roughly a factor of 3 lower with a Druyvesteyn distribution than with a Maxwellian distribution. The densities of the N_2^+, N^+ and N_3^+ ions behave similarly with increasing x, their ratio not changing significantly with x. However, the density of the N_4^+ ion increases somewhat with x, although its density is negligible.

The electron temperature as a function of the electron energy distribution function is shown in figure 12 for various discharge pressures. The behavior of the electron temperature with the varying electron energy distribution function is similar for all the pressures, increasing about 1.3 V at 100 mTorr

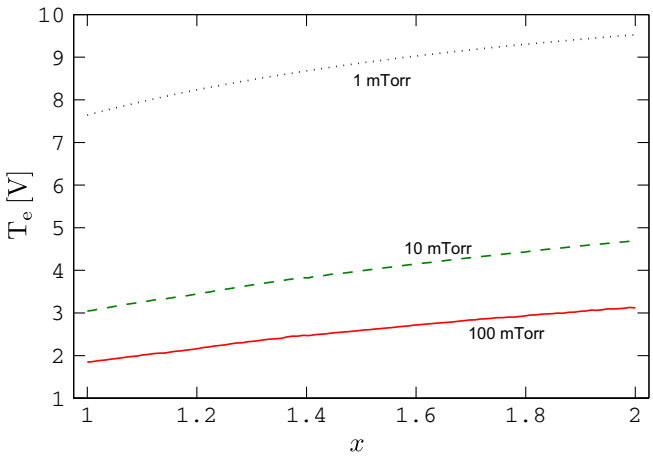

Figure 12. The electron temperature T_e versus the electron energy distribution function for $p = 1$, 10 and 100 mTorr discharge pressure. Conditions are as in figure 11.

and 1.9 V at 1 mTorr when the distribution function is varied from being Maxwellian-like to Druyvesteyn-like. As with the particle densities, the effect of the electron energy distribution function on the electron temperature is not as much as could have been anticipated. This is in fact encouraging since the electron energy distribution function is definitely the most crude assumption we are forced to make in this study.

The relative reaction rates are not shown as a function of the electron energy distribution function in this study since the creation and loss mechanisms are not significantly affected by the varying distribution function. Thus, the creation and destruction mechanisms are fundamentally the same for the Maxwellian-like and Druyvesteyn distributions. Increasing x results mainly in an increasing contribution of wall quenching and recombination. Similar to the evolution of the neutral densities shown in figure 11(*a*), the contribution of processes involving ground state particles increases with increasing x. Meanwhile, the contribution of processes involving particles in excited states decreases accordingly.

Although figure 11(*a*) seems to show a considerable decrease in the dissociation fraction with increasing x, the fraction of the atomic density actually decreases from about 25% to 18%, when the distribution function changes from Maxwellian-like to Druyvesteyn-like. The decrease in the dissociation fraction is even less for other conditions, being almost independent of x when the pressure is 1 mTorr, regardless of the absorbed power. Thus, the electron energy distribution function is certainly not the only reason for a significant overestimation of the atomic density as indicated by a comparison with some of the measurements mentioned in section 3.2.

3.5. Sensitivity to other model parameters

In table 8 we review the relative change in the dissociation fraction $[N]/n_g$, the atomic ion fraction $[N^+]/n_i$, the electron density n_e and the electron temperature T_e with varying gas flow rate Q, gas temperature T_g, wall quenching coefficients γ_Q, wall recombination coefficients γ_{rec} and chamber radius R and length L. The discharge pressure is 10 mTorr, the absorbed power 500 W and the gas flowrate 50 sccm. The chamber is assumed to be cylindrical with the dimensions $R = 10$ cm and $L = 10$ cm and the electron energy distribution function is assumed to be Maxwellian-like.

Table 8. The sensitivity of the plasma parameters to changes in the various model parameters. Values represent the factors of increase or decrease relative to the first value of the range explored for a given model parameter.

Parameter	Range	$[N]/n_g$	$[N^+]/n_i$	n_e	T_e
Q (sccm)	10–1000	↓ 2.1	↓ 1.7	↓ 1.1	1
T_g (K)	300–1200	↑ 1.5	↓ 1.1	↓ 1.4	↑ 1.5
γ_Q	0.01–1	↓ 1.2	↓ 1.6	↓ 1.5	↑ 1.1
γ_{rec}	0.001–1	↓ 14	↓ 5.6	↑ 1.8	1
R (cm)	5–50	↓ 67	↓ 35	↓ 120	↓ 1.2
L (cm)	1–100	↓ 9.6	↓ 4.7[a]	↓ 6.8[a]	↓ 2.3

[a] Peaks at $L = R = 10$ cm before decreasing. See text.

The gas flowrate does not seem to have a strong effect on any of the plasma parameters. While the electron density and electron temperature are almost unaffected, the dissociation fraction and consequently the atomic ion fraction decrease with increasing gas flow, most significantly for flowrates above 100 sccm. Since the total gas density is inversely proportional to the gas temperature, the plasma parameters change similarly with increasing gas temperature as they do with decreasing pressure. The exception to this is the atomic ion fraction which decreases slightly with the increasing temperature, while the dissociation fraction increases. Increasing all the wall quenching coefficients simultaneously towards unity, i.e. for reactions (R58) to (R60), decreases the density of excited species, but only significantly for the metastable atoms and mostly when $\gamma_Q > 0.1$. In fact, the $N_2(X\,^1\Sigma_g^+, v = 1)$ density even increases slightly for $\gamma_Q > 0.1$. The lower metastable atom density results in less total ionization of N^+, decreasing the atomic ion fraction considerably. Although the wall recombination coefficient γ_{rec} has a substantial effect on the ratio of atomic and molecular species, the electron temperature does not change at all. When $\gamma_{rec} < 0.001$ the plasma parameters settle and become independent of the wall recombination coefficient. The dependence of the plasma parameters on the chamber dimensions R and L only demonstrates how important it is to specify the chamber geometry for any measurement in an inductively coupled plasma. While all the plasma parameters decrease uniformly with increasing chamber radius, we found that the densities of metastable atoms and molecules increase with increasing chamber length until the chamber aspect ratio becomes unity, i.e. $L = R = 10$ cm, decreasing steeply for lengths beyond that. This results in an increased total ionization of atoms and a pronounced peak of the atomic ion fraction at $L = 10$ cm which is about 50% larger than the value for $L = 1$ cm. As a consequence, the electron density also increases by roughly 30% before decreasing when $L > R = 10$ cm.

4. Conclusion

A global (volume averaged) model of the nitrogen discharge in the steady state has been developed and deployed to investigate

the dependence of plasma parameters with the discharge pressure. Furthermore, we have evaluated the sensitivity of the result with regard to the choice of the electron energy distribution function. We find that the nitrogen discharge is essentially atomic when the pressure is around 1 mTorr but is highly molecular when the pressure is 100 mTorr. The model calculations of the electron temperature, electron density and ion fractions are in good agreement with measurements. However, our prediction of the density of neutrals, in particular the atomic density, are significantly larger than measured values. This indicates that the dissociation cross section is still questionable, likely being significantly too large, particularly for the dissociation of $N_2(X\,^1\Sigma_g^+, v > 0)$. But any attempts to make the dissociation fraction smaller also result in a smaller atomic ion fraction, which is already in a seemingly good agreement with measurements. The dissociation cross section can therefore not be held solely responsible for the discrepancy between the model calculations and measurements. The density of vibrationally excited ground state molecules $N_2(X\,^1\Sigma_g^+, v > 1)$ is negligible when the pressure is about 1 mTorr but increases rapidly as the pressure is increased, being a substantial part of the total molecular density when the pressure is above 10 mTorr. The choice of the electron energy distribution function has a limited effect on the overall calculation results. Changing the electron energy distribution function from Maxwellian to Druyvesteyn affects mostly the density of excited species, ground state species being more important when the distribution is Druyvesteyn-like. The electron density decreases somewhat with increasing x as well. However, the dissociation fraction is insignificantly affected. Thus, the choice of the electron energy distribution function could in fact be changed to the Druyvesteyn distribution function without changing the agreement with measurements significantly.

Acknowledgments

This work was partially supported by the Icelandic Research Fund, the University of Iceland Research Fund and the Icelandic Research Fund for Graduate Students.

References

[1] Czerwiec T, Greer F and Graves D B 2005 Nitrogen dissociation in a low pressure cylindrical ICP discharge studied by actinometry and mass spectrometry *J. Phys. D: Appl. Phys.* **38** 4278–89

[2] Moustakas T D, Lei T and Molnar R J 1993 Growth of GaN by ECR-assisted MBE *Physica* B **185** 36–49

[3] Tao K, Mao D and Hopwood J 2002 Ionized physical vapor deposition of titanium nitride: a global plasma model *J. Appl. Phys.* **91** 4040–8

[4] Niimi H and Lucovsky G 1999 Monolayer-level controlled incorporation of nitrogen in ultrathin gate dielectrics using remote plasma processing: formation of stacked 'N–O–N' gate dielectrics *J. Vac. Sci. Technol.* B **17** 2610–21

[5] Ishikawa K, Yamaoka Y, Nakamura M, Yamazaki Y, Yamasaki S, Ishikawa Y and Samukawa S 2006 Surface reactions during etching of organic low-k films by plasmas of N_2 and H_2 *J. Appl. Phys.* **99** 083305

[6] Wang L, Ji S and Sun J 2006 Effect of nitriding time on the nitrided layer of AISI 304 austenitic stainless steel *Surf. Coat. Technol.* **200** 5067–70

[7] Shoolib Shah M, Salem M, Ahmad R, Zakaullah M, Qayyum A and Murtaza G 2008 Langmuir probe characterization of nitrogen plasma for surface nitriding of AISI-4140 steel *J. Mater. Process. Technol.* **199** 363–8

[8] Conrad J R, Radtke J L, Dodd R A, Worzala F J and Tran N C 1987 Plasma source ion-implantation technique for surface modification of materials *J. Appl. Phys.* **52** 4591–6

[9] Cho J, Han S, Lee Y, Kim O K, Kim G-H, Kim Y-W, Lim H and Suh M 2001 The measurement of nitrogen ion species ratio in inductively coupled plasma source ion implantation *Surf. Coat. Technol.* **136** 106–10

[10] Lieberman M A and Gottscho R A 1994 Design of high-density plasma sources for materials processing *Physics of Thin Films* vol 18 ed M Francombe and J Vossen (New York: Academic) pp 1–119

[11] Lee C, Graves D B, Lieberman M A and Hess D W 1994 Global model of plasma chemistry in a high density oxygen discharge *J. Electrochem. Soc.* **141** 1546–55

[12] Lee C and Lieberman M A 1995 Global model of Ar, O_2, Cl_2 and Ar/O_2 high-density plasma discharges *J. Vac. Sci. Technol.* A **13** 368–80

[13] Patel K K 1998 Volume averaged modeling of high density discharges *Master's Thesis* Department of Electrical Engineering and Computer Sciences, University of California at Berkeley

[14] Gudmundsson J T, Marakhtanov A M, Patel K K, Gopinath V P and Lieberman M A 2000 On the plasma parameters of a planar inductive oxygen discharge *J. Phys. D: Appl. Phys.* **33** 1323–31

[15] Gudmundsson J T, Kouznetsov I G, Patel K K and Lieberman M A 2001 Electronegativity of low-pressure high-density oxygen discharges *J. Phys. D: Appl. Phys.* **34** 1100–9

[16] Sungjin Kim, Lieberman M A, Lichtenberg A J and Gudmundsson J T 2006 Improved volume-averaged model for steady and pulsed-power electronegative discharges *J. Vac. Sci. Technol.* A **24** 2025–40

[17] Gudmundsson J T, Kimura T and Lieberman M A 1999 Experimental studies of O_2/Ar plasma in a planar inductive discharge *Plasma Sources Sci. Technol.* **8** 22–30

[18] Gudmundsson J T and Thorsteinsson E G 2007 On the role of argon reactions in a low pressure Ar/O_2 discharge *Proc. 28th Int. Conf. on Phenomena in Ionized Gases (Prague, Czech Republic, 15–20 July 2007)* ed J Schmidt *et al* pp 79–82 (Institute of Plasma Physics AS CR, v.v.i.)

[19] Gudmundsson J T and Thorsteinsson E G 2007 Oxygen discharges diluted with argon: dissociation processes *Plasma Sources Sci. Technol.* **16** 399–412

[20] Thorsteinsson E G and Gudmundsson J T 2009 A global (volume averaged) model study of a nitrogen discharge: II. Pulsed power modulation *Plasma Sources Sci. Technol.* **18** 045002

[21] Harmeet Singh and Graves D B 2000 Measurements of the electron energy distribution function in molecular gases in a shielded inductively coupled plasma *J. Appl. Phys.* **88** 3889–98

[22] Singh H and Graves D B 2000 Measurements of the electron energy distribution function in molecular gases in an inductively coupled plasma *J. Appl. Phys.* **87** 4098–106

[23] Amemiya H 1997 Sheath formation criterion and ion flux for non-Maxwellian plasma *J. Phys. Soc. Japan* **66** 1335–8

[24] Gudmundsson T J 2001 On the effect of the electron energy distribution on the plasma parameters of argon discharge: a global (volume averaged) model study *Plasma Sources Sci. Technol.* **10** 76–81

[25] Ashida S, Lee C and Lieberman M A 1995 Spatially averaged (global) model of time modulated high density argon plasma *J. Vac. Sci. Technol.* A **13** 2498–507
[26] Lias S G 2005 Ionization energy evaluation (*NIST Chemistry WebBook, NIST Standard Reference Database* vol 69) ed P J Linstrom and W G Mallard (Gaithersburg MD: National Institude of Standards and Technology)
[27] Yu R, Kramida A E, Reader J and NIST ASD Team 2008 *NIST Atomic Spectra Database* (version 3.1.5) http://physics.nist.gov/asd3
[28] Lofthus A and Krupenie P H 1977 Spectrum of molecular nitrogen *J. Phys. Chem. Ref. Data* **6** 113–307
[29] Bakowski B, Hancock G, Peverall R, Ritchie G A D and Thornton L J 2004 Characterization of an inductively coupled N_2 plasma using sensitive diode laser spectroscopy *J. Phys. D: Appl. Phys.* **37** 2064–72
[30] Tuszewski M 2006 Ion and gas temperatures of 0.46 MHz inductive plasma discharges *J. Appl. Phys.* **100** 053301
[31] Shimada M, Tynan G R and Cattolica R 2006 Rotational and translational temperature equilibrium in an inductively coupled plasma *J. Vac. Sci. Technol.* A **24** 1878–83
[32] Britun N, Gaillard M, Ricard A, Kim Y M, Kim K S and Han J G 2007 Determination of the vibrational, rotational and electron temperatures in N_2 and Ar/N_2 rf discharge *J. Phys. D: Appl. Phys.* **40** 1022–9
[33] Bol'shakov A A, Cruden B A and Sharma S P 2004 Determination of gas temperature and thermometric species in inductively coupled plasmas by emission and diode laser absorption *Plasma Sources Sci. Technol.* **13** 691–700
[34] Biloiu C, Sun X, Harvey Z and Scime E 2007 An alternative method for gas temperature determination in nitrogen plasmas: fits of the bands of the first positive system ($B\,^3\Pi_g \rightarrow A\,^3\Sigma_u^+$) *J. Appl. Phys.* **101** 073303
[35] Linss V, Kupfer H, Peter S and Richter F 2005 Determination of the neutral gas temperature of nitrogen-containing low-pressure plasmas using a two-temperature model *Surf. Coat. Technol.* **200** 1696–701
[36] Thorsteinsson E G 2008 The nitrogen discharge: a global (volume averaged) model study *Master's Thesis* Department of Electrical and Computer Engineering, University of Iceland
[37] Bahati E M, Jureta J J, Belic D S, Cherkani-Hassani H, Abdellahi M O and Defrance P 2001 Electron impact dissociation and ionization of N_2^+ *J. Phys. B: At. Mol. Opt. Phys.* **34** 2963–73
[38] Peterson J R *et al* 1998 Dissociative recombination and excitation of N_2^+: cross sections and product branching ratios *J. Chem. Phys.* **108** 1978–88
[39] Kim Y-K, Irikura K K and Ali M A 2000 Electron-impact total ionization cross sections of molecular ions *J. Res. Natl Inst. Stand. Technol.* **105** 285–91
[40] Deutsch H, Becker K, Defrance P, Onthong U, Parajuli R, Probst M, Matt S and Märk T D 2002 Calculated absolute cross section for the electron-impact ionization of CO_2^+ and N_2^+ *J. Phys. B: At. Mol. Opt. Phys.* **35** L65–9
[41] Cosby P C 1993 Electron-impact dissociation of nitrogen *J. Chem. Phys.* **98** 9544–53
[42] Walter C W, Cosby P C and Helm H 1993 $N(^4S^0)$, $N(^2D^0)$, $N(^2P^0)$ yields in predissociation of excited singlet states of N_2 *J. Chem. Phys.* **99** 3553–61
[43] Dyatko N A, Kochetov I V and Napartovich A P 1993 Electron-energy distribution function in decaying nitrogen plasmas *J. Phys. D: Appl. Phys.* **26** 418–23
[44] Freund R S, Wetzel R C and Shul R J 1990 Measurements of electron-impact-ionization cross sections of N_2, CO, CO_2, CS, S_2, CS_2, and metastable N_2 *Phys. Rev.* A **41** 5861–8
[45] Chen J C Y 1964 Theory of subexcitation electron scattering by molecules. II. Excitation and de-excitation of molecular vibration *J. Chem. Phys.* **40** 3513–20
[46] Dubé L and Herzenberg A 1979 Absolute cross sections from the 'boomerang model' for resonant electron–molecule scattering *Phys. Rev.* A **20** 194–213
[47] Mihajlov A A, Stojanović V D and Petrović Z Lj 1999 Resonant vibrational excitation/de-excitation of $N_2(v)$ by electrons *J. Phys. D: Appl. Phys.* **32** 2620–9
[48] Lieberman M A and Lichtenberg A J 2005 *Principles of Plasma Discharges and Materials Processing* 2nd edn (New York: Wiley)
[49] Feng H, Sun W and Morrison M A 2003 Parameter-free nonadiabatic correlation-polarization potential for vibrational excitation in electron–molecule scattering: application to e–N_2 collisions *Phys. Rev.* A **68** 062709
[50] Itikawa Y 2006 Cross sections for electron collisions with nitrogen molecules *J. Phys. Chem. Ref. Data* **35** 31–53
[51] Ramsbottom C A and Bell K L 1994 Low-energy electron scattering by atomic nitrogen *Phys. Scr.* **50** 666–71
[52] Neynaber R H, Marino L L, Rothe E W and Trujillo S M 1963 Low-energy electron scattering from atomic nitrogen *Phys. Rev.* **129** 2069–71
[53] Piper L G, Holtzclaw K W, Green B D and Blumberg W A M 1989 Experimental determination of the Einstein coefficients for the $N_2(B - A)$ transition *J. Chem. Phys.* **90** 5337–45
[54] Bray K N C 1968 Vibrational relaxation of anharmonic oscillator molecules: Relaxation under isothermal conditions *J. Phys. B: At. Mol. Opt. Phys.* **1** 705–17
[55] Ahn T, Adamovich I V and Lempert W R 2004 Determination of nitrogen V–V transfer rates by stimulated Raman pumping *Chem. Phys.* **298** 233–40
[56] Booth J P and Sadeghi N 1991 Oxygen and fluorine kinetics in electron cyclotron resonance plasmas by time-resolved actinometry *J. Appl. Phys.* **70** 611–20
[57] Phelps A V 1991 Cross-sections and swarm coefficients for nitrogen-ions and neutrals in N_2 and argon ions and neutrals in Ar for energies from 0.1 eV to 10 keV *J. Phys. Chem. Ref. Data* **20** 557–73
[58] Chantry P J 1987 A simple formula for diffusion calculations involving wall reflection and low density *J. Appl. Phys.* **62** 1141–8
[59] Tayal S S and Zatsarinny O 2005 B-spline R-matrix with pseudostates approach for electron impact excitation of atomic nitrogen *J. Phys. B: At. Mol. Opt. Phys.* **38** 3631–45
[60] Hopwood J 1994 Planar RF induction plasma coupling efficiency *Plasma Sources Sci. Technol.* **3** 460–4
[61] Singh H 2000 Experimental studies of inductively coupled plasmas *PhD Thesis* Department of Chemical Engineering, University of California, Berkeley
[62] Zhu X-M and Pu Y-K 2008 Using OES to determine electron temperature and density in low-pressure nitrogen and argon plasmas *Plasma Sources Sci. Technol.* **17** 024002
[63] Agarwal S, Hoex B, van de Sanden M C M, Maroudas D and Aydil E S 2003 Absolute densities of N and excited N_2 in a N_2 plasma *Appl. Phys. Lett.* **83** 4918–20
[64] Aydil E S 2003 personal communication
[65] Shin Y M, Kim E Y and Chung T H 2008 Measurement of the degree of dissociation in inductively coupled nitrogen discharges by using optical emission actinometry and mass spectrometry *J. Korean Phys. Soc.* **53** 617–23
[66] Tian C and Vidal C R 1998 Electron impact ionization of N_2 and O_2: contributions from different dissociation channels of multiply ionized molecules *J. Phys. B: At. Mol. Opt. Phys.* **31** 5369–81
[67] Ristić M, Poparić G B and Belić D S 2007 Rate coefficients for resonant vibrational excitation of N_2 *Chem. Phys.* **331** 410–6
[68] Kim Y-K and Desclaux J-P 2002 Ionization of carbon, nitrogen, and oxygen by electron impact *Phys. Rev.* A **66** 012708

[69] Kossyi I A, Kostinsky A Yu, Matveyev A A and Silakov V P 1992 Kinetic scheme of the non-equilibrium discharge in nitrogen–oxygen mixtures *Plasma Sources Sci. Technol.* **1** 207–20

[70] Gordiets B F, Ferreira C M, Guerra V L, Loureiro J M A H, Nahorny J, Pagnon D, Touzeau M and Vialle M 1995 Kinetic model of a low-pressure N_2–O_2 flowing glow discharge *IEEE Trans. Plasma Sci.* **23** 750–68

[71] Bowers M T, Kemper P R and Laudenslager J B 1974 Reactions of ions in excited electronic states: $(N_2^+\cdot)^* + N_2 \rightarrow N_3^+ + N$ *J. Chem. Phys.* **61** 4394–9

[72] Tatarova E, Dias F M, Gordiets B and Ferreira C M 2005 Molecular dissociation in N_2–H_2 microwave discharges *Plasma Sources Sci. Technol.* **14** 19–31

[73] Herron J T 1999 Evaluated chemical kinetics data for reactions of $N(^2D)$, $N(^2P)$, and $N_2(A\,^3\Sigma_u^+)$ in the gas phase *J. Phys. Chem. Ref. Data* **28** 1453–83

[74] Sugawara K, Ishikawa Y and Sato S 1980 The rate constants of the reactions of the metastable nitrogen-atoms, ^2D and ^2P, and the reactions of $N(^4S) + NO^- \rightarrow N_2 + O(^3P)$ and $O(^3P) + NO + M \rightarrow NO_2 + M$ *Bull. Chem. Soc. Japan* **53** 3159–64

[75] Young R A and Dunn O J 1975 The excitation and quenching of $N(^2P)$ *J. Chem. Phys.* **63** 1150–3

[76] Piper L G 1989 The excitation of $N(^2P)$ by $N_2(A\,^3\Sigma_u^+, v' = 0, 1)$ *J. Chem. Phys.* **90** 7087–95

[77] Piper L G 1989 The excitation of $N_2(B\,^3\Pi_g, v = 1$–$12)$ in the reaction between $N_2(A\,^3\Sigma_u^+)$ and $N_2(X, v \geqslant 5)$ *J. Chem. Phys.* **91** 864–73

[78] Billing G D and Fisher E R 1979 VV-rate and VT-rate coefficients in N_2 by a quantum-classical model *Chem. Phys.* **43** 395–401

[79] Guthrie J A, Chaney R C and Cunningham A J 1991 Temperature dependencies of ternary ion–molecule association reactions yielding N_3^+, N_4^+, and $(CO)_2^+$ *J. Chem. Phys.* **95** 930–6

[80] Piper L G 1993 Reevaluation of the transition-moment function and Einstein coefficients for the $N_2(A\,^3\Sigma_u^+ - X\,^1\Sigma_g^+)$ transition *J. Chem. Phys.* **99** 3174–81

[81] Piper L G 1998 Experimental determination of the Einstein coefficient for the $N(^2P$–$^4S)$ transition *Chem. Phys. Lett.* **296** 397–402

[82] Wiese W L, Fuhr J R and Deters T M 1996 Atomic transition probabilities of carbon, nitrogen, and oxygen—a critical data compilation *J. Phys. Chem. Ref. Data* **25** 1–522

[83] Singh H, Coburn W J and Graves D B 2000 Recombination coefficients of O and N radicals on stainless steel *J. Appl. Phys.* **88** 3748–55

[84] Clark W G and Setser D W 1980 Energy transfer reactions of $N_2(A\,^3\Sigma_u^+)$: V. Quenching by hydrogen halides, methyl halides, and other molecules *J. Phys. Chem.* **84** 2225–33